

# Experimental–Numerical Characterization of the Fracture Behaviour of P264GH Steel Notched Pipes Subject to Internal Pressure

Hassane Moustabchir<sup>1</sup>  · Azari Zitouni<sup>2</sup> · Said Hariri<sup>3</sup> · J. Gilgert<sup>2</sup> · C. I. Pruncu<sup>4</sup>

Received: 9 August 2016 / Accepted: 27 April 2017 / Published online: 16 May 2017  
© The Author(s) 2017. This article is an open access publication

**Abstract** The rupture phenomenon of a mechanical structure requires critical consideration, because of its safety constructions. A detailed experiment of material features as well as the Young's modulus, yield strength, material toughness or fracture resistance provides useful information to predict the life integrity of a pipe structure. This paper presents the most accurate experimental techniques for characterization of a pipe-like structure to assess its reliability. Standard traction tests, dynamic Charpy tests and pressure tests were performed to envisage the crack propagation progress. Detailed information on fracture process was obtained by a robust numerical approach using the finite element method.

**Keywords** Fracture toughness · Stress intensity factor · Volumetric method · Notched pipe

## 1 Introduction

Gas production sites are often very far from consumption centres. To increase the profitability of a pipeline, the use of large tubular structures is appropriate under high pressure. From 1910 to 2000, the diameter of the largest “transport” pipelines was multiplied by 4 and the transport pressure by a value of 60. These increases were possible thanks to great improvements of mechanical properties of the steels used as design tools.

The structural integrity of the pipeline must be guaranteed to avoid any fracture damage. History emphasizes the probability of rupture is never zero. Statistical investigation, established by the European Gas Pipeline Incident Group (Association française pour les règles de conception et de construction des matériels des chaudières électro-nucléaires 1993), identifies 1060 cases of fracture in service between 1970 and 2001. Fifty percentage of these fractures are caused by “external aggression”, and other causes of significant incidents are due to the presence of defects in the material (17%), corrosion (15%) or soil movements (7%).

A simple and very economical tool to predict the pipeline integrity is the volumetric method designed on the notch stress intensity factor concept. The volumetric approach is a semi-local method evaluating the elastoplastic fracture regime based on the numerical configuration of the so-called finite element method (Elminor 2003; Adib and Pluvinaige 2003). This method was firstly applied at the Mechanical Reliability Laboratory of University of Metz. It assumes that the damage processes happening on material to fracture requires a physical volume characterized by an effective distance  $x_{\text{eff}}$ . In that volume, an effective stress is released, acting as an average weight stress surrounded by the stress distribution of the fracture process zone.

✉ C. I. Pruncu  
c.i.pruncu@bham.ac.uk

<sup>1</sup> Équipe Science et Ingénierie des Matériaux (ESIM), Département de Physique, Faculté des Sciences et Techniques Errachidia, Université My Ismaïl, Boutalamine, BP 509, 52000 Errachidia, Morocco  
<sup>2</sup> Laboratoire de Mécanique, Biomécanique, Polymère, Structures (LaBPS), Ecole Nationale d'Ingénieurs de Metz, 1 route d'Ars Laquenexy, 57070 Metz, France  
<sup>3</sup> TPCIM, Ecole des Mines de Douai, 941 rue Charles Bourseul, 59508 Douai Cedex, France  
<sup>4</sup> School of Mechanical Engineering, University of Birmingham, Edgbaston B15 2TT, UK

Originally, Kuguel (1961) suggested taking into account not only the maximum surface stress (hot spot), but also the volume of the core metal stressed at least equal to 95% of the stress surface. An extension of this approach is to apply depth stress characteristic (Neuber 1968), stress at the typical depth (Buch 1974) and the stress gradient (Brand and Sutterlin 1980). Fracture progress follows a cylindrical shape, and its diameter “characteristic distance” is of the order of the grain size for the case of a crack (Ritchie et al. 1973). A critical load, load proportional to the change in the volume, may induce the fracture process (Bermin 1983), while this volume represents the plastic zone. Later on, Barson et al. (1974) and Clark (1974) described the typical distance to be the order of magnitude equal to the radius of notch.

Subsequent studies (Pluvinage et al. 1999; Pluvinage 1998; Boukharouba and Pluvinage 1999) demonstrated that this distance is not linked to the geometry of the notch, but rather to the stress distribution. This distance may relay to a pseudo-stress singularity zone appearing at the  $x_{eff}$  distance from the bottom of the notch. Moreover, this effective distance is the distance from the crack progress to the fracture process zone. Pluvinage (1997) confirmed that the magnitude of the effective stress is less than the magnitude of the maximum stress. The calculation of the stress amplitude must enclose the effects of plastic relaxation.

In order to describe the loading condition or the scale effect (Qylafku 2000), the needs of calculating the stress amplitude from a volume called “volume of fracture process” may be compulsory. The amplitude of the effective stress should consider the state of stress gradient in the volume of fracture process. The importance of this gradient and its role in the rupture initiation point has been reported by various authors (Peterson 1959).

This survey aims to provide a better understanding of how to evaluate the pipeline integrity using the volumetric method designed on the notch stress intensity factor concept. In order to prove the robustness of the present approach, the elastoplastic zone was considered. The results were then validated by detecting the material fracture toughness with a classical dynamic Charpy’s test.

## 2 Computing the Notch Stress Intensity Factor in Mode I

The notch stress intensity factor (NSIF) was accurately determined by Qylafku et al. (1999) considering the volumetric approach, based on the effective stress  $\sigma_{eff}$  and the effective distance  $x_{eff}$ . Boukharouba et al. (1995) and Pluvinage (1997) achieved good results in elastic domain and then extended the analysis to elastic–plastic material behaviour. Qilafku (2001) reveal good progress in determining the NSIF in the “elastoplastic” mode I.

Figure 1 presents the stress distribution computed via FEM analysis following the volumetric approach (VA) tool. There, the elastoplastic stress (opening stress at fracture) and the stress gradient are depicted. This diagram includes four specific areas:

- Zone I* Region close to the initiation point where the elastic–plastic stress, at the crack tip, increases up to the maximum stress. Note that the stress is not maximum at the notch root, but is offset by a certain distance.
- Zone II* The elastic–plastic stress decreases up to the effective distance  $x_{eff}$ .
- Zone III* The evolution of elastoplastic stress has a linear behaviour in the logarithmic chart. This behaviour is expressed by a power law:

$$\sigma_{ij}(\theta) = \frac{K_{\rho}}{(2\pi r)^{\alpha}} f(\theta) \tag{1}$$

where  $K_{\rho}$  is the notch stress intensity factor,  $r$  distance from the initiation point,  $\alpha = 1/2$  (case of a sharp crack),  $\phi$  polar angle.

*Zone IV* This area is far from bottom of the notch and plays no role in the rupture process.

The stress gradient along the x-distance, expressing the influence of stress points on the fracture initiation, is determined:

$$\text{grad}\sigma = \frac{d\sigma}{dx} \tag{2}$$

The effective distance corresponds to a diameter of a cylindrical profile considered as the volume of fracture processes. To determine this effective distance, (Qilafku et al. 2001) used the relative stress gradient, defined as the ratio of the stress gradient and the stress  $\sigma(x)$ :

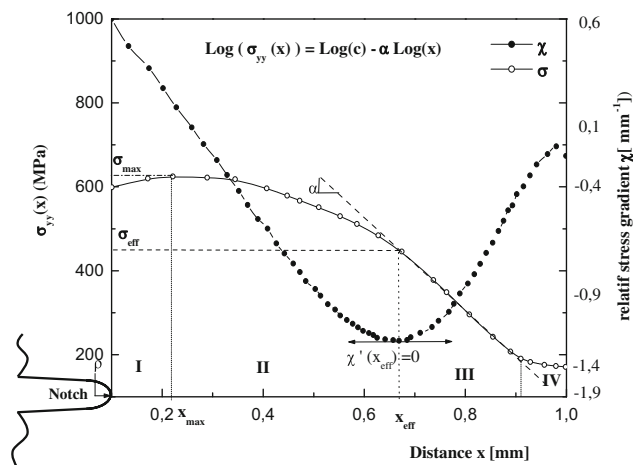


**Fig. 1** Bilogarithmic diagram of the stress distribution  $\sigma_{yy}$  and the gradient elastoplastic stresses obtained by finite element (Qilafku et al. 2001)

$$\chi = \frac{1}{\sigma(x)} \frac{d\sigma(x)}{dx} \tag{3}$$

where  $\chi$  is the gradient relative of stress ( $\text{mm}^{-1}$ ) and  $x$  distance (mm).

The effective stress ( $\sigma_{\text{eff}}$ ) is the weighted average of the stresses enclosed into the volume of the fracture process zone, determined as:

$$\sigma_{\text{eff}} = \frac{1}{x_{\text{eff}}} \int_0^{x_{\text{eff}}} \sigma_{ij}(1 - x\chi) dx \tag{4}$$

The maximum stress intensity factor is determined by:

$$K = \sigma_{\text{eff}} \sqrt{2\pi x_{\text{eff}}} \tag{5}$$

### 3 Experimental Procedure

#### 3.1 Material and Specimens

The material characterization was performed on the P264GH steel specimens. The samples were collected from a pipe having the external diameter of 610 mm and a thickness of 11 mm. That pipeline was used in the 50 s and then removed at the beginning of the twenty-first century. The extracted samples conform to the longitudinal direction ( $L$ ) as depicted in Fig. 2. Their chemical characteristics may differ very little from the standard and are summarized in Table 1.

The microstructure of P264GH steel samples was analysed by optical microscopy after mechanical polishing and chemical treatment with 2% natal. The metallographic analysis confirms that the sheet used in the manufacture of this pipe is rolled in both directions ( $L$  and  $T$ ). We have observed bands of perlite (coloured in black) alternating with bands of ferrite (coloured in white) which is a sign of rolling machining. Figure 3 shows that ferrite is the main component of this microstructure (Fig 4).

The tensile tests were performed at room temperature. For that purpose, six cylindrical specimens of diameter

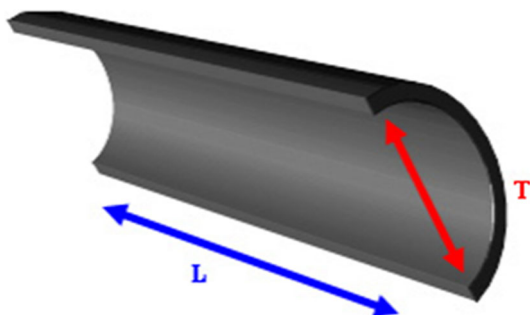


Fig. 2 Longitudinal and transversal directions of a pipeline

7 mm and cross circular section  $S_0$  were machined. These specimens have a total length ( $L_t$ ), an initial length ( $L_0$ ) and a gauge length ( $L_c$ ), as shown in Fig. 3.

With:  $L_0 = k\sqrt{s_0}$ ;  $k = 5, 65$ ;  $L_0 + \frac{d}{2} < L_c < L_0 + 2d$  and  $L_t \geq L_c + 2d$

Figure 5 shows the experimentally determined stress–strain curve. The tested material follows a ductile behaviour.

The main mechanical characteristics obtained are listed in Table 2:

#### 3.2 Dynamical Characterization: Charpy Test

The critical notch stress intensity factor was determined by the Charpy test. The tests were used to characterize the fragility of the material. The main parameter measured was the material resilience which corresponds to the value of energy absorbed per unit of area.

The resilience KCV is defined as the work of fracture per unit of area of the ligament without notch. It is expressed by the critical value of the fracture toughness  $J_{Ic}$  of the energy parameter  $J$ .

Material toughness is proportional to the work of fracture surface. The work of the fracture surface is defined as the work of fracture  $U_c$  per unit of area with the ligament length of  $w.b$ . ( $w$  is the width of the specimen;  $b$  is the ligament) as plotted in Fig. 6. This work of the fracture surface is exactly the resilience rate.

$$KCV = U_c/wb \tag{6}$$

The fracture toughness at the initiation stage may be defined:

$$J_{Ic} = \eta U_c/wb = \eta KCV \tag{7}$$

The proportionality factor  $\eta$  can be determined by two methods:

- Formulae ASTM 813.81 (American standard):  $\eta = 2 + (0.522b/w)$  (8)

- Formulae BS (British standard):  $\eta = 1.97 + (0.518b/w)$  (9)

where  $b$  is the size of ligament sample and  $w$  sample width.

The toughness  $K_{Ic}$  varies depending on the energy absorbed by the standard Charpy V-notch. The fracture toughness  $K_{Ic}$  increases linearly with the energy absorbed by the test Charpy V. A picture with the sample profiles used in these tests is depicted in Fig. 7.

Charpy tests were performed in two different directions as shown in Fig. 7

**Table 1** Chemical composition of P264GH steel sample (wt%)

Material	C	Mn	Si	S	P	Al	Fe
Steel sample tested	0.123	0.665	0.195	0.002	0.013	0.027	Bal.
Steel P264GH according to standard EN 10028.2-92	0.18	1	0.4	0.015	0.025	0.02	Bal.

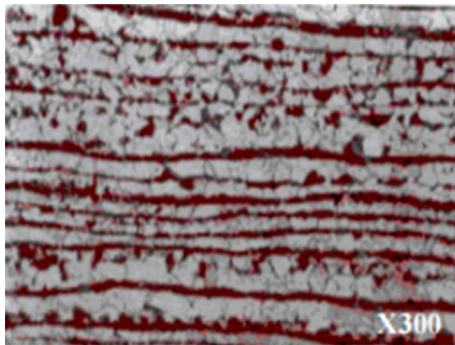


**Fig. 3** A replica of P264GH steel sample microstructure

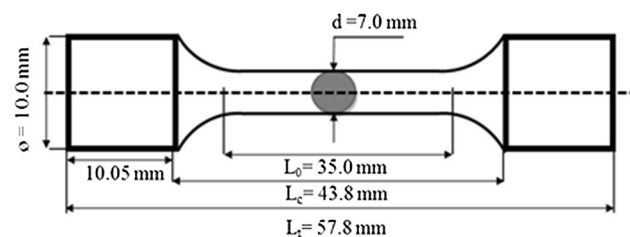


**Fig. 4** Geometry and dimensions of the tensile test specimens

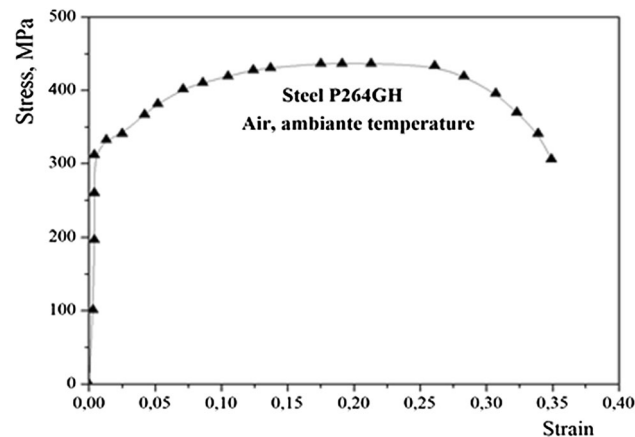


**Fig. 5** Static stress–strain curve of P264GH steel obtained from 1D tensile test

- *L* samples (refers to the longitudinal direction of rolling)
- *T* samples (designates the transverse direction).

The values of the fracture energy for each sample during testing routine are listed in Table 3. The values of the

**Table 2** Mechanical characteristics, at room temperature, of P264GH steel samples

Young’s modulus	$E = 207,000$ MPa
Poisson’s ratio	$\nu = 0.3$
Yield stress	$R_c = 340$ MPa
Ultimate tensile strength	$R_m = 440$ MPa
Elongation to fracture	$A = 35\%$

resilience KCV are determined from Eq. (6), and the fracture toughness  $J_{Ic}$  was obtained from Eq. (7), while the values of the critical notch stresses intensity factor  $K_{Ic}$  were determined as a function of KCV from the curve plotted in Fig. 8.

$$J_{Ic} = \eta K_{Ic} \text{KCV} \tag{10}$$

The value of  $\eta$  was determined by Formula 813.81 ASTM (American Standard):

$$\eta = 2 + (0.522b/w) \tag{11}$$

that gives:

$$\eta_{\text{moy}} = 2, 3.$$

$$K_{Ic} \left[ \text{MPa} \times m^{1/2} \right]$$

The error of the notch stress intensity factor between samples in the transverse direction and in the longitudinal direction, respectively, is only 4%. This indicates that the material is relatively isotropic.

The behaviour of the P264GH steel, subjected to dynamic experiment “Charpy V” test, was analysed, and the potential of material’s ability to absorb the energy until final fracture was assessed from Charpy tests. Experimental results show that the fracture toughness of the samples, in the transverse direction, is closer to the fracture toughness of a standard sample. Material isotropy is more evident in the longitudinal direction.

### 3.3 Study of Defect Harmfulness in the Pressurized Pipe

We performed a rupture test on the structure made of steel “P264GH”. The test used is a “pressurized chamber” with axial default.



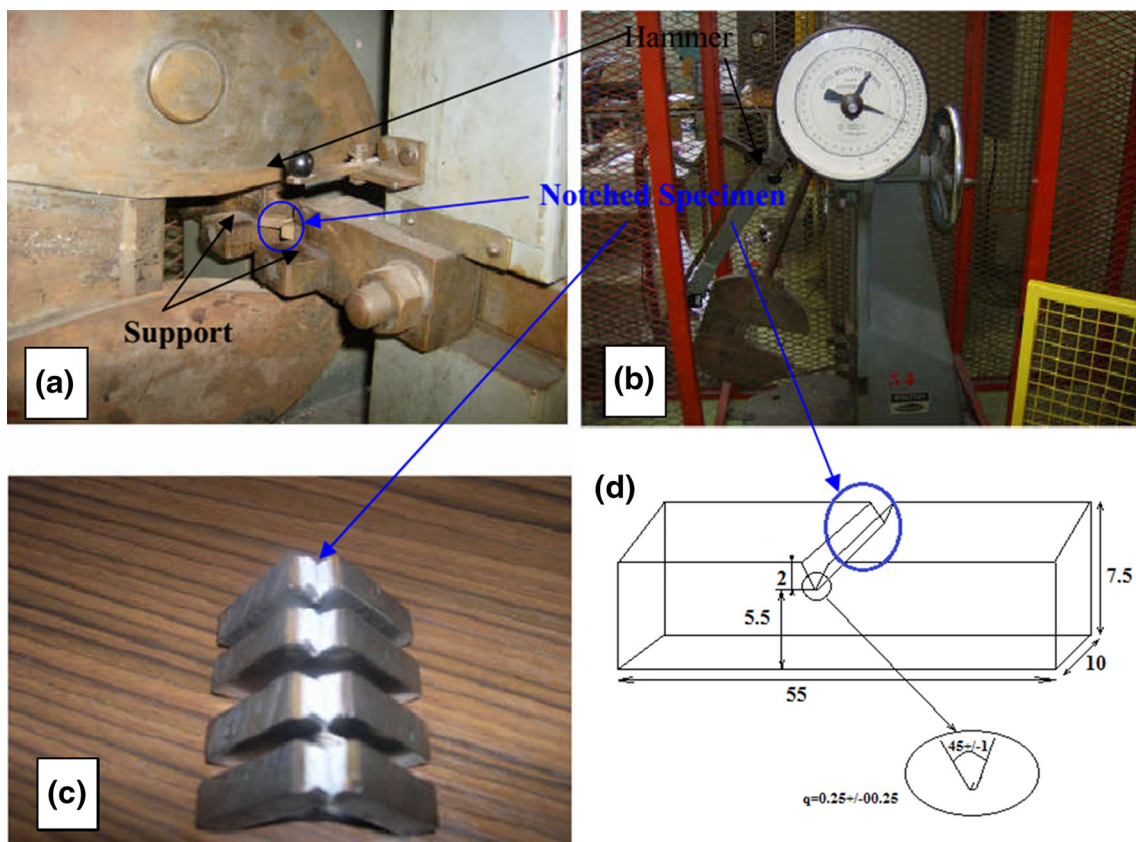


**Fig. 6** Details of entire experiment. **a** Cylindrical shell, **b** Charpy machine used in this study, **c** notched samples after test and **d** details of the geometrical dimensional size of the tested samples with V-notch

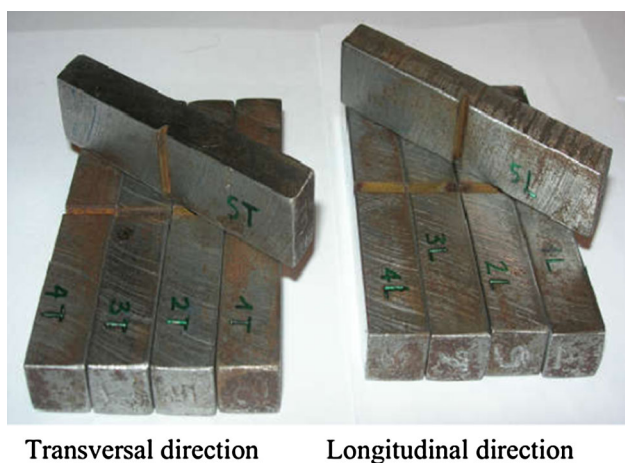


**Fig. 7** Specimens utilized in Charpy impact tests

### 3.3.1 Structural Characterization

The mechanical characterization was performed on a model consisting of a cylindrical shell closed by two types of torispherical head with large radius. The geometry of the

analysed component, selected according to CODAP standard, is shown in detail in Fig. 9. In that study, a longitudinal surface crack that represents a very high risk of pipe fracture during pressurizing (Moustabchir et al. 2016) was considered. Table 4 summarizes the dimensions and orientations of the defect.

The model equipped with the strain gauges was pressurized. The maximum deformation is sensed by the closest strain gauge to the defect.

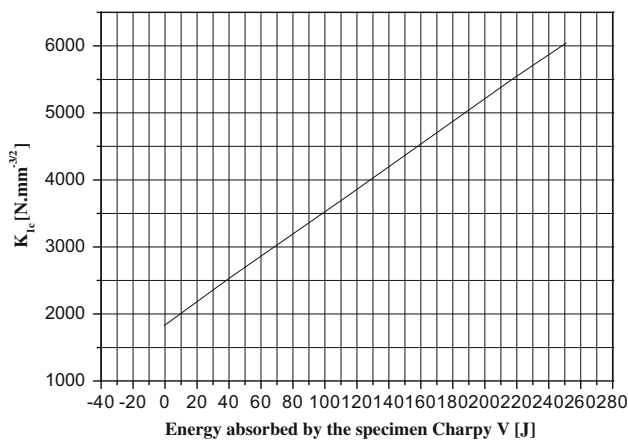
Figure 10 shows the pressure (in bar) as a function of circumferential deformation  $\epsilon_{\theta\theta}$  recorded by the gauge  $J_1, J_2$  situated on the longitudinal chain of the defect C1.

From the curve, relative to the nearest strain gauge to the defect  $D$ , it is possible to see that the deformation zone passes into the plastic range around 40 bar. The data relative to second gauge (located at 4 mm from the defect) indicate that the material enters in the plastic regime at about 43 bar pressure.

In summary, the material becomes more stressed in the vicinity of the defect  $D$ , while the plastic range is obtained for a pressure above 40 bar.

**Table 3** Results of Charpy tests

Number of samples	Energy absorbed at fracture KV (Joules) (Charpy tests)	Energy average KV	Resilience KCV (MJ/m <sup>2</sup> )	Average resilience KCV (MJ/m <sup>2</sup> )	Factor $\eta$	Average factor $\eta$	$J_{Ic}$ (MJ/m <sup>2</sup> )	$J_{Ic}$ average (MJ/m <sup>2</sup> )	NSIF $K_{Ic}$ (MPa m <sup>1/2</sup> )	NSIF average $K_{Ic}$ (MPa m <sup>1/2</sup> )
<i>Transverse direction</i>										
1	86.3	80.54	1.57	1.48	2.29	2.29M	3.59	3.37	102.77	99.13
2	80.2		1.49		2.28		3.39		99.06	
3	74.2		1.4		2.28		3.19		94.87	
4	80		1.48		2.28		3.37		98.82	
5	82		1.44		2.3		3.31		100.14	
<i>Longitudinal direction</i>										
6	64	72.58	1.10	1.27	2.3	2.3	2.53	2.91	90.91	94.99
7	84.1		1.45		2.3		3.33		101.45	
8	76		1.31		2.3		3.01		97.50	
9	67.8		1.23		2.29		2.82		92.23	
10	71		1.24		2.3		2.85		92.89	

**Fig. 8** The notch stress intensity factor  $K_{Ic}$ , as a function of the energy absorbed by the Charpy V piece (British Standards Institution PD 6493 1991)

#### 4 Numerical Analysis of Defect Harmfulness in the Pressurized Pipe

In order to consider the elastoplastic regime, cylindrical shells with outer axisymmetric notch were subjected to an internal pressure of 60 bar (value is consistent with the plastic field, Fig. 10). The model considered was axisymmetric. The notch stress intensity factor was computed at the bottom of defect and then analysed. Its distribution allows detection if the pressure of 60 bar in the elastoplastic domain exceeds the critical stress intensity factor which has been obtained from Charpy's test. Geometric parameters were set as follows:  $alt = 0.2$ ;  $t/R = 0.052$ ;  $c/a = 4$  and  $\rho = 0.25$  mm.

The structures were modelled by CASTEM 2000, in agreement with (Moustabchir et al. 2010, 2012) under

plane strain conditions using free-meshed iso-parametric quadrilateral elements,  $i$ th quarter-point singularity elements at the crack tip. It was enough to model half of the structure because of symmetry in the geometry and loading conditions. The mesh generated from the elastoplastic analyses comprises 31,485 elements and 63,526 nodes. The mesh convergence was achieved for the element size of 2 mm. The FE model utilized in the numerical simulations is illustrated in Fig. 11.

The stress distribution calculated in the elastoplastic region is characterized by a stress relaxation at a distance greater than 0.1 mm from the notch.

Figure 12 shows the distributions of elastoplastic stress, for the 60 bar pressure and for a radius at the bottom of notch  $\rho = 0.25$  mm. The choice of this pressure prevents the elastic case, while we detected that the plastic limit started at 42 bar during the experimental tests.

#### 5 Computing the Notch Stress Intensity Factor by Volumetric Approach

The volumetric approach allows finding the effective distance and effective stress from the diagram of the stress distribution.

In zone II (set as  $r \geq \text{ref}$ ), the stress can be represented by a relation of the type:

$$\sigma_{yy} = \frac{K_{\rho}}{\sqrt{2\pi r}} \quad (12)$$

where  $K_{\rho}$  is the notch stress intensity factor, expressed in MPa (m)<sup>1/2</sup>.

**Fig. 9** a Schematic of the pressurized pipe model and 3D view of the instrumented specimen, b position of the defect, c position of gauge chains near a fault D

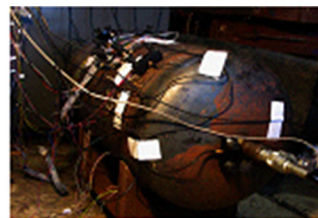
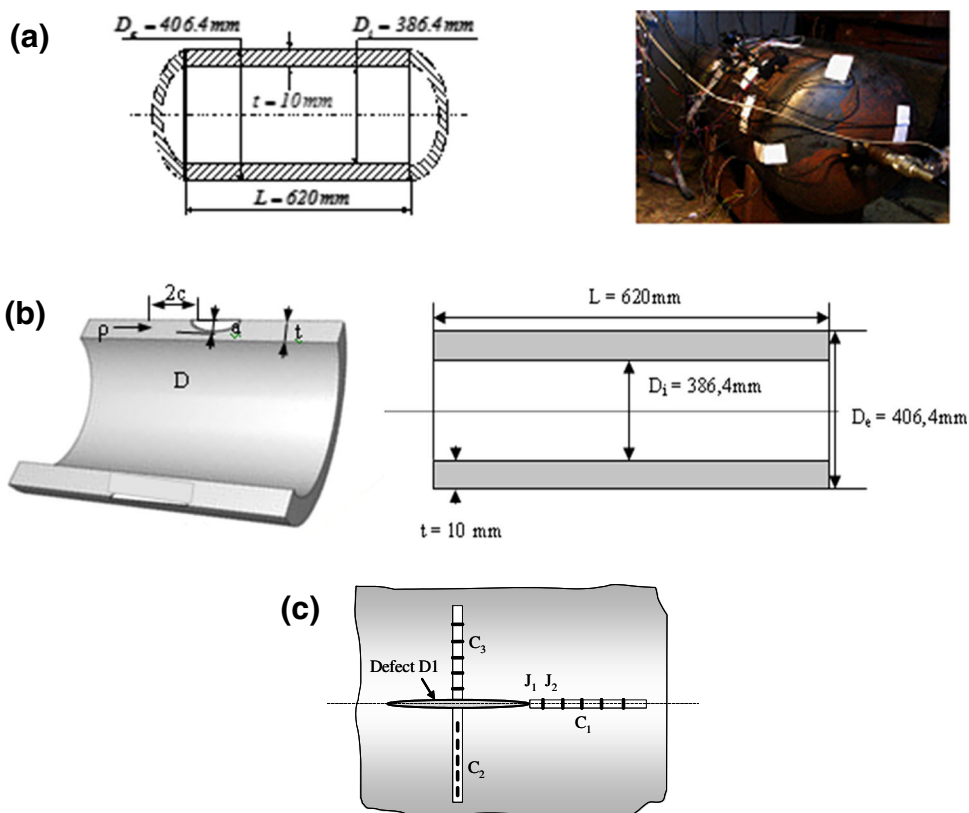


**Table 4** Dimensions of defect studied

Defects	Orientations	Dimensions (mm)
Semi-elliptical (D)	Axial	$a = 2, t = 10$ $c = 8$ $\rho = 0,25$

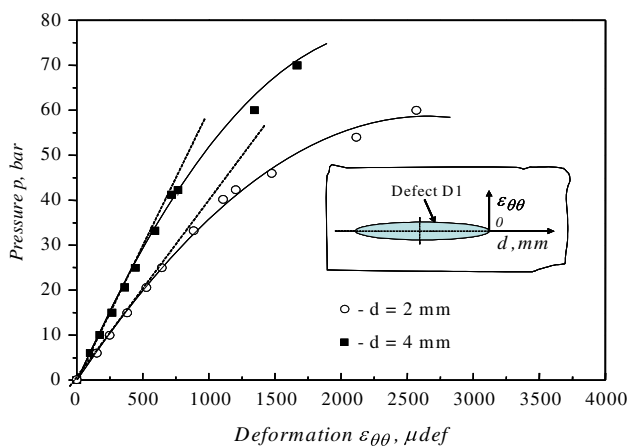


**Fig. 10** Deformation of the gauge ( $J_1, J_2$ ) as a function of the pressure in the case of longitudinal default

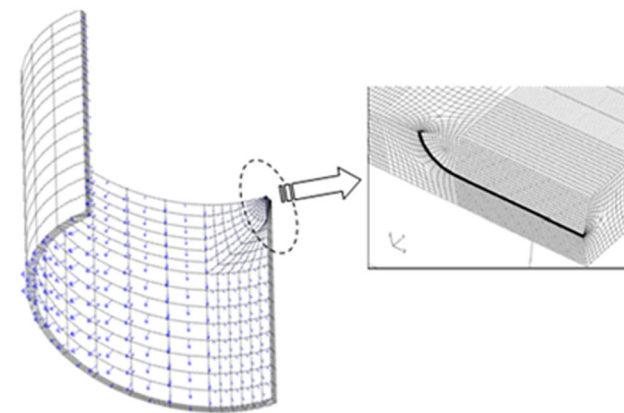


**Fig. 11** A typical mesh adopted in the simulation routine

The equation describing the NSIF in mode I is:

$$\sigma_{yy} = \frac{K_{I\rho}}{\sqrt{2\pi X}} \tag{13}$$

where  $X$  is the distance along the axis of abscissa ( $x$ -axis),  $\sigma_{yy}$  stress in MPa and  $K_{I\rho}$  the notch stress intensity factor in mode I, expressed in MPa ( $m$ )<sup>1/2</sup>. At the boundary of zone II and for  $r = X_{eff}$ , the NSIF, expressed in terms of  $r_{eff}$  and  $\sigma_{eff}$ , becomes:

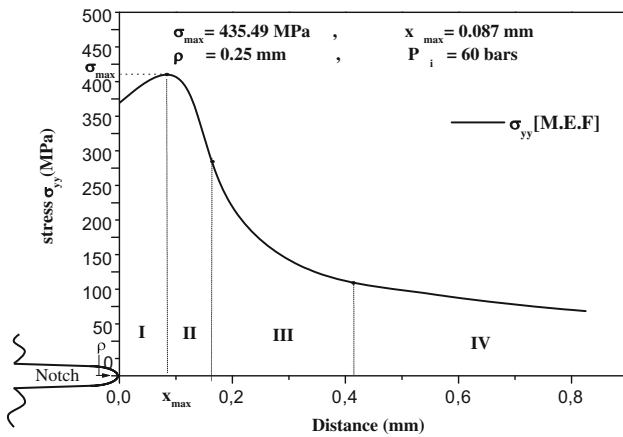


**Fig. 12** Variation of circumferential stress with the distance from the defect computed by elastoplastic FE analysis

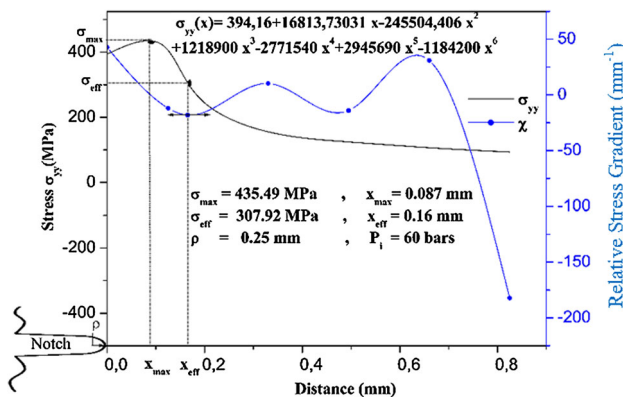


**Fig. 13** Determination of notch stress intensity factor from the volumetric method

$$K_\rho = \sigma_{\text{eff}} \sqrt{2\pi X_{\text{eff}}} \tag{14}$$

Where  $X_{\text{eff}}$  is the effective distance,  $\sigma_{\text{eff}}$  effective stress and  $K_\rho$  the notch stress intensity factor in mode I.

The above equation connected to the stress distribution curve permits determining the relative gradient (see Fig. 13). At the inflection point of this curve, we get the actual distance and the effective stress.

Accurate fitting leads to determine an effective distance of  $X_{\text{eff}} = 0.16$  mm corresponding to an effective stress of 307.92 MPa.

The volumetric method allows the  $K_{I\rho}$  to be calculated as follows:

$$K_\rho = 307.92 \sqrt{2\pi \cdot 0.16 \times 0.001}$$

That gives:

$$K_\rho = 9,76 \text{ MPa } (m^{1/2})$$

## 6 Conclusion

Charpy’s test is a very robust methodology for accurately detecting the material behaviour even in the presence of small modifications. When linear fracture mechanics was developed, a radical revision was introduced. In 1970, the impact testing procedure was improved using the fracture toughness parameter under the impact test in terms of critical stress intensity factor/critical strain energy release rate. However, regardless of all these variants, Charpy’s test remains one of the best experimental solutions to verify the consistency of the materials for structural applications.

This study investigated the mechanical behaviour of notched steel pipes subject to internal pressure. The characterization in terms of fracture toughness was performed in both directions (i.e. longitudinal/transversal), demonstrating the isotropy of P264GH steel.

Numerical simulations were specifically developed for the elastoplastic regime where the evolution of the stress distribution is a nonlinear function. Despite an applied pressure of 60 bar, the notch stress intensity factor calculated for the case of a longitudinal crack remains low. Computed values of NSIF are very conservative. This indicates that the 60 bar pressure considered in the simulations does not exceed the critical stress intensity factor determined by Charpy tests.

**Open Access** This article is distributed under the terms of the Creative Commons Attribution 4.0 International License (<http://creativecommons.org/licenses/by/4.0/>), which permits unrestricted use, distribution, and reproduction in any medium, provided you give appropriate credit to the original author(s) and the source, provide a link to the Creative Commons license, and indicate if changes were made.

## References

Adib H, Pluvillage G (2003) Theoretical and numerical aspects of the volumetric approach for fatigue life prediction in notched components. *Int J Fatigue* 25:67–76

Association française pour les règles de conception et de construction des matériels des chaudières électro-nucléaires (1993) RCC-MR, Règles de conception et de construction des matériels mécaniques des îlots nucléaires RNR: 2e modificatif, mai 1993 [à l’] éd. juin 1985, Règles de conception et de construction des centrales électro-nucléaires. AFCEN. ISSN:0763-2797

Barson JM, McNicol RC (1974) Effect of stress concentration on fatigue crack initiation in Hy-130 steel. *ASTM STP* 559:pp 183–204

Bermin FM (1983) *Metall. Transaction* 14A:2287–2296

Boukharouba T, Pluvillage G (1999) Prediction of semi-elliptical defect form, case of a pipe subjected to internal pressure. *Nucl Eng Des* 188(2):161–171

Boukharouba T, Tamine Niu L, Chehimi C, Pluvillage G (1995) The use of notch stress intensity factor as a fatigue crack initiation parameter. *Eng Fract Mech* 52:503–512



- Brand A, Sutterlin R (1980) Calcul des pièces à la fatigue. Méthode du gradient. Publication Cotin, Senlis
- British Standards Institution PD 6493 (1991) Guidance on some methods for the derivation of acceptance levels for defects in fusion welded joints. British Standards Institution, London
- Buch A (1974) Analytical approach to size and notch size effects in fatigue of aircraft of material specimens. *Mater Sci Eng* 15:75–85
- Clarck WG Jr (1974) Evaluation of the fatigue crack initiation properties of type 403 stainless steel in air and stress environments. In: *Fracture toughness and slow-stable cracking*. ASTM STP 559, American Society for Testing and Materials, pp 205–224
- Elminor H (2003) Fracture toughness of high strength steel (using the notch stress intensity and volumetric approach). *Struct Saf* 25:35–45
- Kuguel R (1961) A relation between theoretical stress concentration factor and fatigue notch factor deduced from the concept of highly stress volume. *Proc ASTM* 61:732–748
- Moustabchir H, Azari Z, Hariri S, Dmytrakh I (2010) Experimental and numerical study of stress–strain state of pressurized cylindrical shells with external defects. *Eng Fail Anal* 17:506–514
- Moustabchir H, Azari Z, Hariri S, Dmytrakh I (2012) Experimental and computed stress distribution ahead of a notch in a pressure vessel: application of T-stress conception. *Comput Mater Sci* 58:59–66
- Moustabchir H, Pruncu CI, Azari Z, Hariri S, Dmytrakh I (2016) Fracture mechanics defect assessment diagram on pipe from steel P264GH with a notch. *Int J Mech Mater Des* 12:273–284
- Neuber H (1968) Theoretical determination of fatigue strength at stress concentration, Air force materials laboratoire, report AFML-TR, 68-20
- Peterson RE (1959) Notch sensitivity. In: Sines G, Waisman JL (eds) *Metal fatigue*. McGraw Hill, New York, pp 293–306
- Pluvinage G (1997) Rupture et fatigue d'amorçées à partir d'entaille—Application du facteur d'intensité de contrainte. *Revue Française de Mécanique*, pp 53–61, No 1997-1
- Pluvinage G (1998) Fatigue and fracture emanating from notch; the use of the notch stress intensity factor. *Nucl Eng Des* 185(2–3):173–184
- Pluvinage G, Azari Z, Kadi N, Dlouhý I, Kozák V (1999) Effect of ferritic microstructure on local damage zone distance associated with fracture near notch. *Theor Appl Fract Mech* 31(2):149–156
- Qilafku G, Kadi N, Dobranski J, Azari Z, Gjonaj M, Pluvinage G (2001) Fatigue of specimens subjected to combined loading. Role of hydrostatic pressure. *Int J Fatigue* 23(8):689–701
- Qylafku G (2000) Effet d'entaille en fatigue de grand nombre de cycles effet du gradient.7 Mémoire de thèse doctorat d'université de Metz
- Qylafku G, Azari Z, Kadi N, Gjonaj M, Pluvinage G (1999) Application of a new model proposal for fatigue life prediction on notches and key-seats. *Int J Fatigue* 21:753–760
- Ritchie RO, Knott JF, Rice JR (1973) On the relationship between critical tensile stress and fracture toughness in mild steel. *J Mech Phys Solids* 21:395–410